IOP Conf. Series: Journal of Physics: Conf. Series **878** (2017) 012018 doi:10.1088/1742-6596/878/1/012018

Chiral symmetry restoration versus deconfinement in heavy-ion collisions at high baryon density

E. L. Bratkovskaya[1,2], A. Palmese[3], W. Cassing[3], E. Seifert[3], T. Steinert[3], and P. Moreau[1]

[1] Institute for Theoretical Physics, University of Frankfurt, Frankfurt, Germany
[2] GSI Helmholtzzentrum für Schwerionenforschung GmbH, Darmstadt, Germany
[3] Institute for Theoretical Physics, University of Giessen, Giessen, Germany

Abstract. The effect of the chiral symmetry restoration (CSR) on observables from heavy-ion collisions is studied in the energy range $\sqrt{s_{NN}}$=3–20 GeV within the Parton-Hadron-String Dynamics (PHSD) transport approach. The PHSD includes the deconfinement phase transition as well as essential aspects of CSR in the dense and hot hadronic medium, which are incorporated in the Schwinger mechanism for the hadronic particle production. We adopt different parametrizations of the nuclear equation of state from the non-linear $\sigma - \omega$ model, which enter in the computation of the quark scalar density for the CSR mechanism, in order to estimate the uncertainty in our calculations. For the pion-nucleon Σ-term we adopt $\Sigma_\pi \approx$ 45 MeV which corresponds to some 'world average'. Our systematic studies show that chiral symmetry restoration plays a crucial role in the description of heavy-ion collisions at $\sqrt{s_{NN}}$=3–20 GeV, realizing an increase of the hadronic particle production in the strangeness sector with respect to the non-strange one. We identify particle abundances and rapidity spectra to be suitable probes in order to extract information about CSR, while transverse mass spectra are less sensitive. Our results provide a microscopic explanation for the "horn" structure in the excitation function of the K^+/π^+ ratio: the CSR in the hadronic phase produces the steep increase of this particle ratio up to $\sqrt{s_{NN}} \approx 7$ GeV, while the drop at higher energies is associated to the appearance of a deconfined partonic medium.

1. Introduction

The main goal of heavy-ion collision (HIC) physics is the study of nuclear matter at high temperatures and/or high densities. According to Quantum-Chromo-Dynamics (QCD), at large temperatures and densities the hadrons cannot survive anymore as bound states and they dissolve forming the Quark-Gluon-Plasma (QGP). At Relativistic Heavy-Ion Collider (RHIC) energies for the first time the creation of a QGP, identified as an almost perfect fluid, has been proven experimentally. Actually, the properties of this deconfined state of matter are still debated as well as the phase boundaries to the hadronic phase. In order to shed some light on this issue, many heavy-ion experiments are performed at the Super-Proton Synchrotron (SPS), RHIC, the Large Hadron Collider (LHC) and will be performed at the future Facility for Antiproton and Ion Research (FAIR) as well as the Nuclotron-based Ion Collider fAcility (NICA). The crucial challenge is to identify in the final particle distributions those signatures, which allow to disentangle the QGP contribution that is impossible to observe directly or independently.

The strange particle production has always been suggested as one of the most sensitive observables that could spot out the creation of a QGP during the early stages of a HIC. The

earliest suggested signature is the strangeness enhancement in A+A collisions with respect to elementary p+p collisions [1, 2]. Later on, Gazdzicki and Gorenstein [3] proposed that a sharp rise and drop in the excitation function of the K^+/π^+ ratio (so called "horn") should show up due to the appearance of a QGP phase at a center-of-mass energy $\sqrt{s_{NN}} \sim 7\,\mathrm{GeV}$ [2]. Several statistical models [4, 5, 6] have succeeded in reproducing the trend of the experimental observation of the K^+/π^+ ratio and other strange to non-strange particle ratios, but they can provide only a statistical description of the heavy-ion collision process. On the other hand there was no conclusive interpretation of the "horn" from dynamical approaches for HIC, like microscopic transport models [7, 8, 9]. Only recently, the Parton-Hadron-String Dynamics (PHSD), a transport approach describing HIC on the basis of partonic, hadronic and string degrees-of-freedom, obtained a striking improvement on this issue when including chiral symmetry restoration (CSR) in the string decay for hadronic particle production [10, 11].

Apart from deconfinement the chiral symmetry restoration addresses another aspect of the QCD phase diagram in the (T, μ_B)-plane as an additional transition between a phase with broken and a phase with restored chiral symmetry. As in case of the QCD deconfinement phase transition, the boundaries of the CSR phase transition line are not well known. Lattice QCD (lQCD) calculations show that at vanishing baryon chemical potential μ_B=0 the CSR takes place at roughly the same critical temperature and energy density as the deconfinement phase transition which is a crossover. At finite baryon chemical potential lQCD calculations cannot be performed due to the sign problem and one must rely on effective models (or extrapolations) in order to study the QCD phase transitions [12, 13, 14, 15, 16]. Different models support the idea that at finite chemical potential a partially restored phase is achieved before the deconfinement occurs [17, 18, 19]. In order to distinguish the two phases of such a transition, effective models use the scalar quark condensate $\langle\bar{q}q\rangle$ as an order parameter. As the baryon density and temperature increase, the scalar quark condensate $\langle\bar{q}q\rangle$ is expected to decrease from a non-vanishing value in the vacuum to $\langle\bar{q}q\rangle \approx 0$ which corresponds to CSR. Since $\langle\bar{q}q\rangle$ is not a measurable quantity, it is crucial to determine experimental observables which are sensitive to this feature. Since long the dilepton spectroscopy has been in the focus in this respect since in a chirally restored phase the spectral functions of the the ρ- and the a_1-meson should become identical. However, no clear evidence has been achieved so far [20]. On the other hand, the strangeness production at Alternating-Gradient Synchrotron (AGS) and lower SPS energies was suggested to be a signature of CSR [10].

In this contribution we will report on the main results from Refs. [10, 11] where a systematic study has been performed on effects of the CSR on final particle distributions within the PHSD approach.

2. Reminder of the PHSD transport approach

The Parton-Hadron-String Dynamics (PHSD) is a microscopic covariant dynamical approach for strongly interacting systems in and out-of equilibrium [21, 22, 23]. It is a transport approach which goes beyond the quasi-particle approximation, since it is based on Kadanoff-Baym equations for the Green's functions in phase-space representation in first-order gradient expansion [24, 25]. Including both a hadronic and a partonic phase as well as a transition between the effective degrees-of-freedom, PHSD is capable to describe the full time evolution of a relativistic heavy-ion collision. The theoretical description of the partonic degrees-of-freedom (quarks and gluons) is realized in line with the Dynamical-Quasi-Particle Model (DQPM) [25] which reproduces lQCD results in thermodynamical equilibrium and provides the properties of the partons, i.e. masses and widths in their spectral functions. In equilibrium the PHSD reproduces the partonic transport coefficients such as shear and bulk viscosities or the electric

[2] In this work we adopt natural units, hence $\hbar = c = 1$.

conductivity from lQCD calculations as well. For a review on PHSD we refer the reader to Ref. [26]. We further note that the pure hadronic phase in PHSD is equivalent to the Hadron-Strings Dynamics (HSD) model [27]. Accordingly, the comparison between PHSD and HSD calculations allows us to disentangle the role of the QGP phase in heavy-ion collisions.

The PHSD approach has been tested for different colliding systems (p+p, p+A, A+A) in a wide range of bombarding energy, from AGS to LHC energies, and has been able to describe a large number of experimental observables, such as charged particle spectra, collective flow coefficients v_n as well as electromagnetic probes such as photons and dileptons [26]. More recently, it has been also shown to provide a microscopic description of the maximum in the K^+/π^+ ratio in central nucleus-nucleus collisions [10, 11].

2.1. String fragmentation in PHSD

The string formation and decay represents the dominant particle production mechanism in nucleus-nucleus collisions for bombarding energies from 2 AGeV to 160 AGeV. In PHSD, the primary hard scatterings between nucleons are described by string formation and decay in the FRITIOF Lund model [28]. A string is an excited color-singlet state, which is composed of two string ends corresponding to the leading constituent quarks of the colliding hadrons and a color flux tube in between. As the string ends recede, virtual $q\bar{q}$ or $qq\bar{q}\bar{q}$ pairs are produced in the uniform color field, causing the breaking of the string. Finally, the string decays into mesons or baryon-antibaryon pairs with formation time $\tau_f \sim 0.8\,\mathrm{fm/c}$ (in the rest-frame of the string).
In the string decay, the flavor of the produced quarks is determined via the Schwinger formula [29], which defines the production probability of massive $s\bar{s}$ pairs with respect to light flavor production ($u\bar{u}, d\bar{d}$) pairs:

$$\frac{P(s\bar{s})}{P(u\bar{u})} = \frac{P(s\bar{s})}{P(d\bar{d})} = \gamma_s = \exp\Big(-\pi\frac{m_s^2 - m_{u,d}^2}{2\kappa}\Big)\,, \tag{1}$$

with $\kappa \approx 0.176\,\mathrm{GeV}^2$ representing the string tension and $m_{u,d,s}$ denoting the constituent quark masses for strange and light quarks. For the constituent quark masses $m_u \approx 0.35\,\mathrm{GeV}$ and $m_s \approx 0.5\,\mathrm{GeV}$ in the vacuum, the production of strange quarks is suppressed by a factor of $\gamma_s \approx 0.3$ with respect to the light quarks, which is the default setting in the FRITIOF routines.

2.2. Modeling of the chiral symmetry restoration

In Refs. [10, 11] the PHSD has been extended to include CSR in the string decay in a hadronic environment of finite baryon and meson density. Here we recall the main aspect of this extension which is based on the Hellman-Feynman theorem for the scalar quark condensate [30]. Accordingly, a linear decrease of the scalar quark condensate $\langle\bar{q}q\rangle$ – which is nonvanishing in the vacuum due to a spontaneous breaking of chiral symmetry – is expected with baryon density ρ_B towards a chiral symmetric phase characterized by $\langle\bar{q}q\rangle \approx 0$ [31, 32]. This decrease of the scalar quark condensate is expected also to lead to a change of the hadron properties with density and temperature, i.e. in a chirally restored phase the vector and axial vector currents should become equal [33]; the latter implies that e.g. the ρ and a_1 spectral functions should become identical (as addressed above in the context of dilepton production). Since the scalar quark condensate $\langle\bar{q}q\rangle$ is not a direct observable, its manifestations should also be found indirectly in different hadronic abundances and spectra or particle ratios like K^+/π^+, $(\Lambda + \Sigma^0)/\pi^-$ etc. as advocated in Ref. [10].

In leading order the scalar quark condensate $\langle\bar{q}q\rangle$ can be evaluated in a dynamical calculation as follows [34]:

$$\frac{\langle\bar{q}q\rangle}{\langle\bar{q}q\rangle_V} = 1 - \frac{\Sigma_\pi}{f_\pi^2 m_\pi^2}\rho_S - \sum_h \frac{\sigma_h \rho_S^h}{f_\pi^2 m_\pi^2}\,, \tag{2}$$

where σ_h stands for the σ-commutator of the relevant mesons h, $\langle\bar{q}q\rangle_V$ represents the vacuum condensate, $\Sigma_\pi \approx 45\,\mathrm{MeV}$ is the pion-nucleon Σ-term and f_π and m_π are the pion decay constant and pion mass, respectively.

In Eq. (2), the quantities ρ_S and ρ_S^h denote the nucleon scalar density and the scalar density for a meson of type h, respectively. The scalar density of mesons h is evaluated in the independent-particle approximation as:

$$\rho_S^h(x) = \frac{(2s+1)(2\tau+1)}{(2\pi)^3}\int \mathrm{d}^3p \frac{m_h}{\sqrt{\mathbf{p}^2+m_h^2}} f_h(x,\mathbf{p})\,, \tag{3}$$

where $f_h(x,\mathbf{p})$ denotes the meson phase-space distribution ($x = (\mathbf{r},t)$) and s,τ refer to the discrete spin and isospin quantum numbers, respectively. Moreover, the vacuum scalar condensate $\langle\bar{q}q\rangle_V = \langle\bar{u}u\rangle_V + \langle\bar{d}d\rangle_V \approx 2\langle\bar{u}u\rangle_V$ can be computed according to the Gell-Mann-Oakes-Renner (GOR) relation [35, 36],

$$f_\pi^2 m_\pi^2 = -\frac{1}{2}(m_u^0 + m_d^0)\langle\bar{q}q\rangle_V\,, \tag{4}$$

and gives $\langle\bar{q}q\rangle_V \approx -3.2\,\mathrm{fm}^{-3}$ for the bare quark masses $m_u^0 = m_d^0 \approx 7\,\mathrm{MeV}$. Finally, in Eq. (2) the nucleon scalar density ρ_S has to be determined in a suitable model with interacting degrees-of-freedom in order to match our knowledge on the nuclear EoS at low temperature and finite density. A proper (and widely used) approach is the non-linear $\sigma-\omega$ model for nuclear matter where ρ_S is defined as:

$$\rho_S(x) = \frac{d}{(2\pi)^3}\int \mathrm{d}^3p \frac{m_N^*}{\sqrt{\mathbf{p}_N^{*2}+m_N^{*2}}} f_N(x,\mathbf{p})\,, \tag{5}$$

where m_N^* and p_N^* denote the effective mass and momentum, respectively, and $f_N(x,\mathbf{p})$ the phase-space occupation of a nucleon while the degeneracy factor is d=4. In fact, in the non-linear $\sigma-\omega$ model the nucleon mass is modified due to the scalar interaction with the medium:

$$m_N^*(x) = m_N^v - g_s\sigma(x)\,, \tag{6}$$

where m_N^v denotes the nucleon mass in vacuum and $\sigma(x)$ is the scalar field which mediates the interaction between the nucleons and the medium with the coupling g_s. In order to calculate ρ_S, we need to determine the value of the scalar field $\sigma(x)$ at each space-time point x. This is done via the non-linear gap equation [37, 38]:

$$m_\sigma^2\sigma(x) + B\sigma^2(x) + C\sigma^3(x) = g_s\rho_S(x) = g_s d\int \frac{\mathrm{d}^3p}{(2\pi)^3}\frac{m_N^*(x)}{\sqrt{\mathbf{p}^2+m_N^{*2}}} f_N(x,\mathbf{p})\,, \tag{7}$$

since for matter at rest we have $\mathbf{p}^* = \mathbf{p}$. In Eq. (7) the self-interaction of the σ-field is included up to the forth order. The parameters g_s, m_σ, B, C are fixed in order to reproduce the values of the nuclear matter quantities at saturation, i.e. the saturation density, the binding energy per nucleon, the compression modulus, and the effective nucleon mass. Actually, there are different sets for these quantities (NL1,NL2,NL3) that lead to slightly different saturation properties. For details we refer the reader to Ref. [11].

The main idea in Ref. [10] is to consider effective masses for the dressed quarks in the Schwinger formula (1) for the string decay in a hot and dense medium. The effective quark

masses can be expressed in terms of a scalar coupling to the quark condensate $\langle\bar{q}q\rangle$ in first order as follows:

$$m_s^* = m_s^0 + (m_s^v - m_s^0)\frac{\langle\bar{q}q\rangle}{\langle\bar{q}q\rangle_V}\,, \qquad\qquad m_q^* = m_q^0 + (m_q^v - m_q^0)\frac{\langle\bar{q}q\rangle}{\langle\bar{q}q\rangle_V}\,, \tag{8}$$

with $m_s^0 \approx 100\,\mathrm{MeV}$ and $m_q^0 \approx 7\,\mathrm{MeV}$ for the bare quark masses. In Eq. (8) the effective masses decrease from the vacuum values with decreasing scalar condensate $\langle\bar{q}q\rangle$ to the constituent masses. This adaptation of the Schwinger formula in case of a hot and dense medium implies a modification of the flavor production factors in Eq. (1). In an actual nucleus-nucleus collision, PHSD incorporates a dynamical calculation of all these features for each cell in space-time:

- the scalar density ρ_S is determined by solving the gap equation (7) for the σ-field;
- the scalar condensate $\langle\bar{q}q\rangle$ is then computed via Eq. (2);
- the effective masses m_q^*, m_s^* are calculated according to Eqs. (8) and plugged in the Schwinger formula (1) in order to compute the flavor production ratios for the string decay.

We stress that, once the nucleon scalar density ρ_S and $\Sigma_\pi(\approx 45$ MeV) are fixed, there is no additional 'parameter' in the PHSD3.3 compared to the previous version PHSD3.2 that has been employed for a couple years for the analysis of relativistic heavy-ion reactions [26]. We note that the sets NL1 and NL3 have the same compression modulus K but differ in the effective mass m^*/m at saturation density whereas NL1 and NL2 have the same effective mass but differ in the compression modulus K. By comparing the results from NL1, NL2 and NL3 we will be able to explore separately the effects from the effective mass and compression modulus. For a detailed discussion of the flavor ratio γ_s versus energy density for the different parameter sets NL1, NL2 and NL3 we refer the reader to Ref. [11]. We only recall that in the partonic phase the s/u ratio remains constant as a function of the energy density since the strings are no longer formed in the QGP.

3. Application to nucleus-nucleus collisions

In this section we present results for the rapidity distribution of the most abundant particles at AGS and SPS energies for different nuclear equations of state in order to estimate the uncertainties of our approach. In addition we also explore the impact of CSR on the transverse dynamics by calculating the transverse mass spectra for protons, pions, kaons and antikaons in comparison to available data. We recall that in particular the transverse slopes of the kaon spectra had been clearly underestimated in the earlier HSD studies (without a partonic phase) [8].

3.1. Rapidity spectra at AGS and SPS energies

We present in Fig. 1 the PHSD results for the rapidity distribution of protons, $(\Lambda + \Sigma^0)$'s, pions and kaons for central nucleus-nucleus collisions at different energies (from AGS to top SPS energies) in comparison to the experimental data from Refs. [39, 40, 41, 42]. The following scenarios will be explored at different energies:

- default PHSD calculations without CSR, represented by the dotted blue lines;
- PHSD calculations including CSR with NL3 as parameter set for the nuclear EoS, represented by the solid red lines;
- PHSD calculations including CSR with NL1 as parameter set for the nuclear EoS, represented by the dashed green lines.

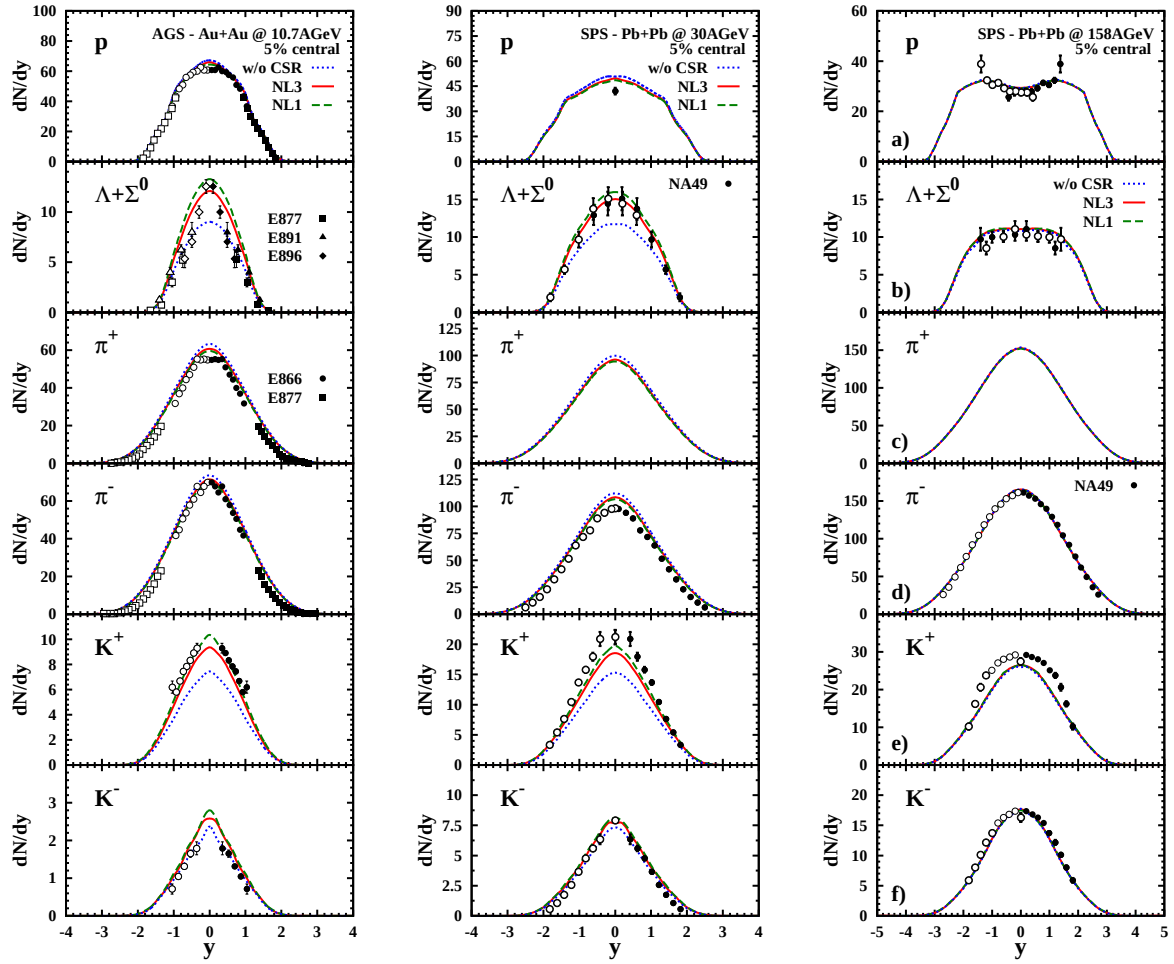

Figure 1. (l.h.s.) The rapidity distribution of protons, $(\Lambda + \Sigma^0)$'s, pions and kaons for 5% central Au+Au collisions at 10.7 AGeV in comparison to the experimental data from Refs. [39, 40]. The solid (red) lines show the results from PHSD including CSR with NL3 parameters, the dashed green lines show the results from PHSD including CSR with NL1 parameters and the blue dotted lines show the result from PHSD without CSR. (middle panel) The rapidity distribution of protons, $(\Lambda+\Sigma^0)$'s, pions and kaons for 5% central Au+Au collisions at 30 AGeV in comparison to the experimental data from Ref. [41]. (r.h.s.) The rapidity distribution of protons, $(\Lambda+\Sigma^0)$'s, pions and kaons for 5% central Au+Au collisions at 158A GeV in comparison to the experimental data from Ref. [42].

We note that PHSD calculations for the parameter set NL2 are not shown explicitly since the results are in between those for NL1 and NL3 [11].

First, we compare the results with and without CSR at $E_{Lab} = 10.7$ AGeV (Fig. 1, l.h.s.), to point out the general effect of this mechanism on the final particle rapidity distributions and in particular show the dependence on the parameter sets NL1 and NL3 for the non-linear $\sigma - \omega$ model for the nuclear EoS. The restoration of chiral symmetry gives an enhancement of the strange particle yields both for mesons and baryons. On the other hand, it produces a slight decrease in the number of pions at midrapidity due to the suppression of pions in the string decays in favor of strange hadrons. The proton rapidity spectra do not present any sensible variation, in fact the CSR as implemented in PHSD modifies essentially the chemistry

of the newly produced particles in the string decay and has a minor impact the dynamics of the nucleons, which in the string picture are associated to the string ends of the primary interactions in the system. The inclusion of the CSR is essential in order to correctly reproduce the strange particle rapidity spectra, as we can see especially for $(\Lambda + \Sigma^0)$ hyperons and K^+ mesons. Furthermore, our calculations for the proton rapidity spectra are in good agreement with experimental observation.

Next, we discuss the results from PHSD with CSR using two different parametrization for the nuclear equation of state, i.e. NL3 and NL1. The general features of the strangeness enhancement hold for both parametrizations; in particular the NL1 set provides larger values for all strange particle rapidity spectra at midrapidity since the scalar nucleon density is larger in this case. The difference between the two parametrizations represents the uncertainty of our results related to CSR as implemented in PHSD.

In Fig. 1 (middle panel) the rapidity spectra of various hadrons at $E_{Lab} = 30\,\mathrm{AGeV}$ are shown. We find the same features as for $E_{Lab} = 10.7\,\mathrm{AGeV}$ concerning the strangeness enhancement and the comparison between the two parameter sets for the equation of state; the differences are slightly smaller at this energy. At midrapidity, both protons and pions are very slightly over-estimated in all explored scenarios which suggests that the nuclear stopping is still a bit overestimated. Finally, at the top SPS energy $E_{Lab} = 158\,\mathrm{AGeV}$ (Fig. 1, r.h.s.) the CSR does not play a significant role, since the dynamics is dominated by the QGP phase. Thus, there is no appreciable difference between the results with and without CSR for the two different EoS. Our results for K^+ are lower with respect to the experimental data, however, the $(\Lambda + \Sigma^0)$, π^- and K^- as well as the protons are correctly reproduced. It is presently unclear where these final differences stem from, since strangeness conservation is exactly fulfilled in the PHSD calculations.

3.2. Transverse mass spectra at AGS and SPS energies

We recall that in earlier HSD calculations (without a partonic phase) the slopes of the transverse mass distributions have been severely underestimated [8]. In Fig. 2 we display the transverse mass spectra for pions and kaons in central Au+Au collisions at AGS energies (l.h.s.) and in Pb+Pb collisions at SPS energies (r.h.s.), respectively. We focus on the role played by the CSR on the mesons transverse mass spectra. At the lower energies, $E_{Lab} = 2\,\mathrm{AGeV}$ there is no appreciable difference between the calculation with and without CSR, since the energy density reached by the system is not high enough to produce a vanishing scalar quark condensate. Instead, in the energy range $E_{Lab} = 4 - 40\,\mathrm{AGeV}$, we notice a small difference between the scenarios with and without CSR. As already mentioned, the CSR acts directly on the chemistry and not so much on the dynamics of the Schwinger mechanism, thus the effect of the partial restoration of chiral symmetry is rather small on the transverse mass spectra. The kaon spectra are harder when CSR is included, while the pion spectra remain essentially unchanged. At the higher SPS energies $E_{Lab} = 80, 158\,\mathrm{AGeV}$ the dynamics of the system is ruled dominantly by the QGP phase and our calculations do not show any sensitivity on the inclusion of CSR. The agreement of our PHSD calculations with the data in Fig. 2 is good in all cases studied.

3.3. Strange particle abundances and ratios

In this subsection we study the excitation function of the particle ratios K^+/π^+, K^-/π^- and $(\Lambda + \Sigma^0)/\pi$ at midrapidity from 5% central Au+Au collisions. In Fig. 3 (l.h.s.) we show the calculations for the following three scenarios: the default PHSD without CSR (blue dotted line), PHSD including CSR with NL3 and NL1 as parameter sets for the nuclear EoS from the non-linear $\sigma - \omega$ model (red solid and green dashed lines, respectively). The shaded area displays the uncertainties of our calculations from the two scenarios for the nuclear EoS since the results from the parameter set NL2 are always in between those from NL1 and NL3 [11].

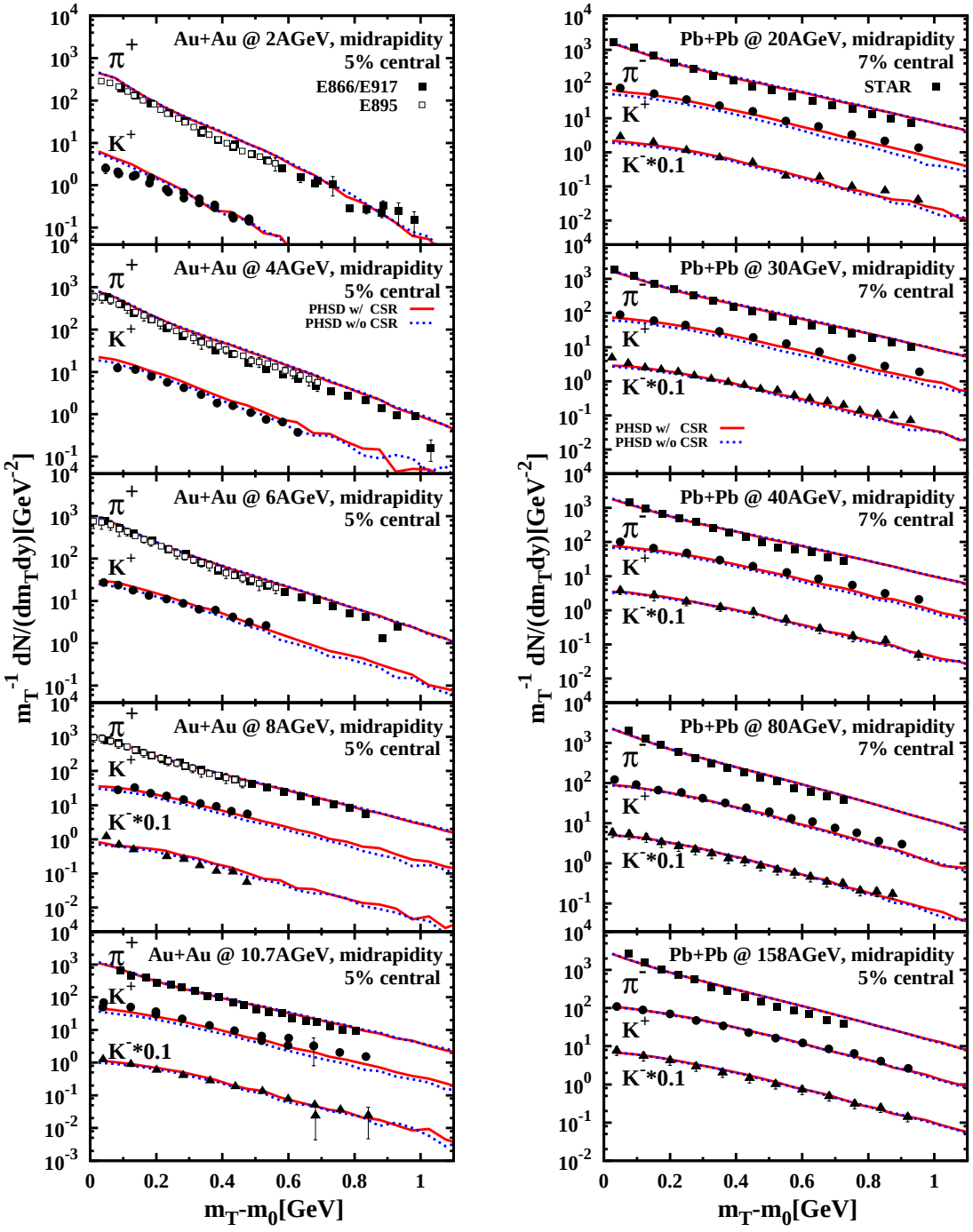

Figure 2. (l.h.s.) The transverse mass spectra of pions and kaons for 5% central Au+Au collisions at $2, 4, 6, 8, 10.7$ AGeV in comparison to the experimental data from Refs. [43, 44]. We show the results from PHSD including CSR with NL3 parameters by solid (red) lines and those from PHSD without CSR by dotted (blue) lines. (r.h.s.) The transverse mass spectra of pions and kaons for 5% and 7% central Pb+Pb collisions at $20, 30, 40, 80, 158$ AGeV in comparison to the experimental data from Ref. [45].

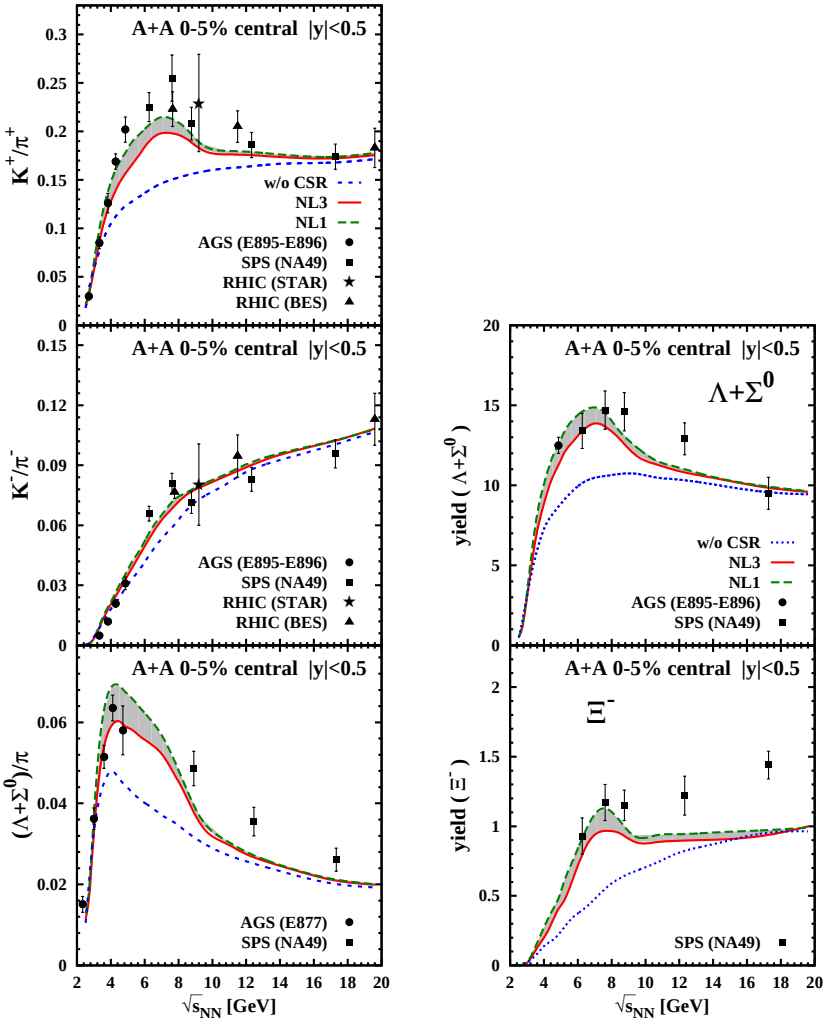

Figure 3. (l.h.s.) The ratios K^+/π^+, K^-/π^- and $(\Lambda+\Sigma^0)/\pi$ at midrapidity from 5% central Au+Au collisions as a function of the invariant energy $\sqrt{s_{NN}}$ up to the top SPS energy in comparison to the experimental data from [44, 46, 47]. The coding of the lines is the same as in Fig. 1. The grey shaded area represents the results from PHSD including CSR taking into account the uncertainty from the parameters of the $\sigma-\omega$-model for the EoS. (r.h.s.) The yields of $(\Lambda+\Sigma^0)$ and Ξ^- at midrapidity from 5% central Au+Au collisions as a function of the invariant energy $\sqrt{s_{NN}}$ up to the top SPS energy in comparison to the experimental data from Refs. [40, 47].

As described in Ref. [10], the inclusion of CSR in PHSD is responsible for the strong strangeness enhancement at AGS and low SPS energies. The experimental observations of the ratios K^+/π^+ and $(\Lambda+\Sigma^0)/\pi$ show the well-known "horn" structure, which is reproduced by the PHSD calculations with CSR. In fact, CSR gives rise to a steep increase of these ratios at energies lower than $\sqrt{s_{NN}} \approx 7\,\mathrm{GeV}$, while the drop at larger energies is associated to the appearance of a deconfined partonic medium. The NL1 parameter set produces a sharper peak both in the K^+/π^+ and in the $(\Lambda+\Sigma^0)/\pi$ excitation functions with a $\approx 10\%$ maximum increase with respect to the NL3 result. We point out that even adopting different parametrizations for the $\sigma-\omega$ model, we recover the same "horn" feature. This supports the reliability of the CSR

mechanism as implemented in the PHSD model.

At AGS energies, the energy dependencies of the ratios K^+/π^+ and $(\Lambda + \Sigma^0)/\pi$ are closely connected, since K^+ and Λ (or Σ^0) are mostly produced in pairs due to strangeness conservation. On the other hand, the excitation function of the K^-/π^- ratio does not show any peak, but smoothly increases as a function of $\sqrt{s_{NN}}$. In fact, especially at AGS energies, the antikaon production differs substantially from the production of K^+ and Λ, which occurs predominantly via string formation. In fact, the antikaons are produced dominantly via secondary meson-baryon interactions by flavor exchange and their production is suppressed with respect to the Λ hyperons that carry most of the strange quarks. This is the reason why the inclusion of chiral symmetry restoration provides a substantial enhancement of the K^+/π^+ and $(\Lambda + \Sigma^0)/\pi$ excitation functions and a smaller change on the K^-/π^- ratio. We also notice that there is no sizeable difference between the NL1 and NL3 results for the K^-/π^- ratio. At top SPS energies the strangeness is produced predominantly by the hadronization of partonic degrees-of-freedom, thus our results for all the ratios do not show an appreciable sensitivity to the nuclear EoS and the calculations with and without CSR tend to merge at $\sqrt{s_{NN}} \approx 20\,\mathrm{GeV}$.

Finally, in Fig. 3 (r.h.s.) we present the yields of $(\Lambda + \Sigma^0)$ and Ξ^- at midrapidity from 5% central Au+Au collisions as a function of the invariant energy $\sqrt{s_{NN}}$ in comparison to the available data from Refs. [40, 47]. We recover a "horn" structure, similar to that shown in Fig. 3 (l.h.s.) for the energy dependence of the strange to non-strange particle ratios. A sensitivity on the nuclear model parametrizations persists at low energy, while in the top SPS energy regime the results corresponding to the different scenarios merge. The comparison with the available data at $\sqrt{s_{NN}} < 8\,\mathrm{GeV}$ supports the validity of the CSR picture, while at larger energies we under-estimate the experimental observations. We mention that this discrepancy is not due to the CSR mechanism, since it does not play an essential role in the high-energy regime as pointed out above.

4. Summary

We point out that our PHSD calculations provide a microscopic interpretation of the "horn" structure in the excitation function of the K^+/π^+ ratio in central Au+Au (or Pb+Pb) collisions. The steep rise of this ratio at AGS energies is associated to chiral symmetry restoration (CSR), while the drop at higher SPS energies is due to the appearance of the QGP phase in an increasing volume of the interaction region. We have found an analogous energy dependence for the $(\Lambda + \Sigma^0)/\pi$ ratio, while the excitation function of the K^-/π^- ratio does not show any explicit peak. In general, the PHSD results obtained with the inclusion of CSR are in a good agreement with the available data for all observables analyzed, while calculations without CSR fail substantially.

The microscopic PHSD studies support the idea that CSR occurs in hadronic systems with high temperatures and densities before the deconfinement phase transition takes over. We suggest that the strange particle spectra and yields are suitable signatures to study the properties of CSR in HICs in future also as a function of system size and centrality as advocated in Ref. [11].

Acknowledgments

The authors acknowledge inspiring discussions with J. Cleymans, M. Gazdzicki, M. Gorenstein and O. Linnyk and thank the Helmholtz International Center for FAIR (HIC for FAIR), the Helmholtz Graduate School for Hadron and Ion Research (HGS-HIRe), the Helmholtz Research School for Quark Matter Studies in Heavy-Ion Collisions (H-QM), and the Bundesministerium für Bildung und Forschung (BMBF) for support. The computational resources have been provided by the LOEWE-CSC.

References

[1] Rafelski J and Müller B 1982 *Phys. Rev. Lett.* **48** 106
[2] Stock R 2002 *J. Phys.* **G 28** 1517
[3] Gazdzicki M and Gorenstein M I 1999 *Acta Phys. Polon.* **B 30** 2705
[4] Cleymans J *et al.* 2005 *Phys. Lett.* **B 615** 50
[5] Andronic A Braun-Munzinger P and Stachel J 2009 *Phys. Lett.* **B 673** 142
[6] Bugaev K A *et al.* 2013 *Europhys. Lett.* **104** 22002
[7] Geiss J Cassing W and Greiner C 1998 *Nucl. Phys.* **A 644** 107
[8] Bratkovskaya E L *et al.* 2004 *Phys. Rev.* **C 69** 054907
[9] Bratkovskaya E L Soff S Stöcker H van Leeuwen M and Cassing W 2004 *Phys. Rev. Lett.* **92** 032302
[10] Cassing W Palmese A Moreau P and Bratkovskaya E L 2016 *Phys. Rev.* **C 93** 014902
[11] Palmese A *et al.* 2016 *Phys. Rev.* **C 94** 044912
[12] Senger P *et al.* 2011 *Lect. Notes Phys.* **814** 681
[13] Fischer C S Luecker J and Welzbacher C 2014 *Phys. Rev.* **D 90** 034022
[14] Fischer C S Fister L Luecker J and Pawlowski J M 2014 *Phys. Lett.* **B 732** 273
[15] Eichmann G Fischer C S and Welzbacher C 2016 *Phys. Rev.* **D 93** 034013
[16] Herbst T K Pawlowski J M and Schaefer B J 2013 *Phys. Rev.* **D 88** 014007
[17] McLerran L and Pisarski R D 2007 *Nucl. Phys.* **A 796** 83
[18] Nambu Y and Jona-Lasinio G 1961 *Phys. Rev.* **122** 345
[19] Klevansky S P 1992 *Rev. Mod. Phys.* **64** 649
[20] Rapp R 2013 *Adv. High Energy Phys.* **2013** 148253
[21] Cassing W and Bratkovskaya E L 2009 *Nucl. Phys.* **A 831** 215
[22] Bratkovskaya E L Cassing W Konchakovski V P and Linnyk O 2011 *Nucl. Phys.* **A 856** 162
[23] Konchakovski V P *et al.* 2012 *Phys. Rev. C* **85** 044922
Konchakovski V P *et al.* 2012 *Phys. Rev.* **C 85** 011902
[24] Kadanoff L P and Baym G 1962 *Quantum Statistical Mechanics*, Benjamin, New York
[25] Cassing W 2009 *Eur. Phys. J. ST* **168** 3
Cassing W 2007 *Nucl. Phys.* **A 795** 70
[26] Linnyk O Bratkovskaya E and Cassing W 2016 *Prog. Part. Nucl. Phys* **87** 50
[27] Cassing W and Bratkovskaya E L 1999 *Phys. Rep.* **308** 65
[28] Andersson B Gustafson G and Pi H 1993 *Z. Phys.* **C 57** 485
[29] Schwinger J 1951 *Phys. Rev.* **83** 664
[30] Cohen T D Furnstahl R J and Griegel D K 1992 *Phys. Rev.* **C 45** 1881
[31] Vogl U and Weise W 1991 *Prog. Part. Nucl. Phys.* **27** 195
[32] Birse M C 1994 *J. Phys.* **G 20** 1537
[33] Koch V 1997 *Int. J. Mod. Phys.* **E 6** 203
[34] Friman B Nörenberg W and Toneev V D 1998 *Eur. Phys. J.* **A 3** 165
[35] Bando M Kugo T and Yamawaki K 1988 *Phys. Rep.* **164** 217
[36] Cohen T D Furnstahl R J Griegel D K and Jin X 1995 *Prog. Part. Nucl. Phys.* **35** 221
[37] Boguta J and Bodmer A R 1977 *Nucl. Phys.* **A 292** 413
[38] Lang A *et al.* 1991 *Z. Phys.* **A 340** 287
[39] Stachel J 1996 *Nucl. Phys.* **A 610** 509C
[40] Albergo S *et al.* 2002 *Phys. Rev. Lett.* **88** 062301
[41] Alt C *et al.* 2008 *Phys. Rev.* **C 77** 024903 2006 *Phys. Rev.* **C 73** 044910 2008 *Phys. Rev.* **C 78** 034918
[42] Afanasiev S V *et al.* 2002 *Phys. Rev.* **C 66** 054902
Anticic T *et al.* 2011 *Phys. Rev.* **C 83** 014901 2012 *Phys. Rev.* **C 86** 054903
[43] Ahle L *et al.* 2000 *Phys. Lett.* **B 476** 1 (2000) 1998 *Phys. Rev.* **C 58** 3523
[44] Klay J L *et al.* 2003 *Phys. Rev.* **c 68** 054905
[45] Alt V *et al.* 2004 *J. Phys.* **G 30** 119 2008 *Phys. Rev.* **C 77** 024903
Afanasiev S V *et al.* 2002 *Phys. Rev.* **C 66** 054902
[46] Abelev B I *et al.* 2010 *Phys. Rev.* **C 81** 024911
Aggarwal M M *et al.* 2011 *Phys. Rev.* **C 83** 024901
[47] Alt C *et al.* 2008 *Phys. Rev.* **C 78** 034918